



Inert-living matter, when cells and beads play together

Usharani Nagarajan^{1,8}, Grégory Beaune^{1,5,8}, Andy Y. W. Lam ^{1,6,7}, David Gonzalez-Rodriguez ²,
Françoise M. Winnik^{1,3,8} & Françoise Brochard-Wyart^{4,8}✉

While both active and granular matter have been extensively studied, here we investigate what happens when we mix the two of them, in a model system combining microparticles and cell assemblies. On a substrate covered with polystyrene or silica microparticles, we notice two regimes in the spreading of a cell aggregate: light particles are pushed by the cells and form a ring, which bonds to the substrate by adhesion forces that oppose spreading, while for heavy particles, the cell monolayer spreads above the particle bed. In both cases, cell activity is transmitted to inert beads, leading to the formation of cell-microparticle aggregates, which flicker and diffuse. We then study the formation and the spreading of hybrid aggregates of microparticles and living cells and observe phase separations and jamming transitions. Our study may have implications on processes such as cancer metastasis and development, and may guide cancer therapies based on inert particles.

¹International Center for Materials Nanoarchitectonics (MANA), National Institute for Materials Science, 1-1 Namiki, Ibaraki, Tsukuba 305-0044, Japan. ²Université de Lorraine, LCP-A2MC, F-57000 Metz, France. ³Department of Chemistry, University of Helsinki, FI-00014 Helsinki, Finland. ⁴Institut Curie, Université PSL, Sorbonne Université, CNRS UMR168, Laboratoire Physico Chimie Curie, 75005 Paris, France. ⁵Present address: Department of Applied Physics, Aalto University School of Science, Puumiehenkuja 2, 02150 Espoo, Finland. ⁶Present address: Institute for Quantitative Biosciences, The University of Tokyo, Bunkyo-ku, Tokyo 113-0032, Japan. ⁷Present address: Department of Computational Biology and Medical Sciences, Graduate School of Frontier Sciences, The University of Tokyo, Bunkyo-ku, Tokyo 113-0032, Japan. ⁸These authors contributed equally: Usharani Nagarajan, Grégory Beaune, Françoise M. Winnik, Françoise Brochard-Wyart. ✉email: Francoise.Brochard@curie.fr

Flocks of birds, aggregates of ants, live tissues, modular robots, and active colloids belong to the broad field of “Active Matter”, which describes the collective behavior of systems maintained in non-equilibrium states by a constant input of energy. Unlike swarms of fish and flocks of birds, cells can support static loads because they are bound by transient links. The transient nature of the links leads to viscoelastic behaviors. The concept of “Entangled active matter” has emerged recently to provide a unified understanding of the behavior of swarms of adhesive motile particles¹. Live tissues are elastic and relax like rubbers at short times and flow like liquids at long times, a property of long entangled polymer chains. Even if cells are not as sensitive to thermal agitation, they consume energy and produce a large noise, which allows them to flow.

Cell aggregates are among the simplest examples of entangled active matter. Increasingly, biologists, pharmacologists, and toxicologists use them as substitutes to animal studies². They are reliable systems for drug screening, bridging the gap between 2D cell-based assays and animal studies. In the field of tissue engineering, cell aggregates are commonly used as building blocks implanted in vivo for organ reconstruction, raising the hope of eventually replacing costly organ transplant procedures^{3,4}.

Cell aggregates also play an important role in fundamental studies of the properties and functions of active matter. For example, they are used to study cooperative collective migration and spreading⁵. Their behavior follows universal laws of soft matter physics⁶. For example, the spreading of cell aggregates on a substrate is analogous to the spreading of a viscous droplet: upon contact with an adhesive substrate, the aggregate flattens and surrounds itself by a cellular monolayer named precursor film⁷.

Mixed aggregates consisting of two cell types spontaneously segregate, so that the most cohesive cells (highest surface tension) occupy the core of the aggregate and the least cohesive cells surround them^{8,9}, very much like immiscible liquids. Mixture of active self-propelling colloidal particles also segregate, with the « hot » particles (high velocities) surrounding the « cold » ones¹⁰.

On the other hand, inert particles of size comparable to that of the cell do not move like Brownian particles and belong to the field of granular matter: at rest, they behave like a solid, such as a heap of sand, because thermal fluctuations are too weak to overcome the energy barrier between different conformations of the particle distribution. While the glass transition in polymer liquids occurs upon cooling, the jamming transition of granular materials occurs upon increasing the volume fraction, which controls mechanical stability. At high volume fraction, the crowding of beads prevents them from flowing under applied stress, which corresponds to a solid state. As the volume fraction is decreased, the system may be able to flow, which corresponds to a liquid state.

The fields of granular matter and active matter are both under intensive investigation, and the dynamics and mechanical properties of granular materials as well as those of cell aggregates are reasonably well understood. However, much less is known about the mixture of inert and active matter. We introduce here another level of complexity by combining cell aggregates and microparticles (MPs), thus raising several questions.

For example, how do cell aggregates spread on a carpet of passive MPs? Two cases are observed depending upon the size of the MPs. Small MPs are phagocytosed¹¹. MPs too large to be internalized by the cells are put into Brownian-like motion by the migrating cells, in analogy to MPs activated by bacteria¹².

Is it possible to assemble hybrid aggregates containing live cells and inert MPs, such as polymer MPs? Whereas nanoparticles have been used to stick cells together¹³, how will large particles similar in size to the cells co-aggregate? To the best of our knowledge, the concept is new in the context of entangled active

matter, where little is known about the dynamics of assemblies of live and inert particles. Interestingly, Campas et al. introduced liquid droplets (~5–600 μm) in cell aggregates and used their deformation as a sensor to quantify cell-generated mechanical forces¹⁴. A hybrid cell aggregate is possibly the simplest model of “hybrid active matter”. Studies in this direction may not only have profound implications on our understanding of active matter, but also physiological applications in tissue engineering and cancer invasion¹⁵.

How are the wetting properties modified by the presence of MPs? For aggregates of cells, the key parameter is the sign of the spreading parameter $S = W_{CS} - W_{CC}$, where W_{CS} and W_{CC} are the cell-substrate and cell-cell adhesion energies, respectively⁵. If $S < 0$ ($W_{CS} < W_{CC}$), which corresponds to the regime of “partial wetting”, the aggregate does not spread. If $S > 0$ ($W_{CS} > W_{CC}$), which corresponds to the regime of “complete wetting”, the aggregate spreads with the formation of a precursor film¹⁶. For aggregates spreading on a carpet of MPs, S depends on the size, density, and surface fraction of the MPs. For hybrid aggregates spreading on fibronectin-coated glass substrates, both the cohesion (W_{CC}) and the level of adhesion with the substrate (W_{CS}) will depend upon their composition. Moreover, as in the spreading of binary mixtures, phase separation may be coupled to spreading, and the MP volume fractions in the film and in the aggregate may be different¹⁷.

How are the mechanical properties of the aggregate modified by the presence of inert MPs? The MPs alone do not flow, but it is possible to induce a jamming transition by varying the cell volume fraction. The dynamics of spreading of hybrid aggregates of MPs and cells will reflect the change of mechanical properties with aggregate composition. Because tissues are composite materials made of cells and extracellular matrix, hybrid aggregates mimic living matter better than simpler cell aggregates do. The extracellular matrix is composed of proteins secreted by the cells themselves. The chemical composition and the rigidity of the extracellular matrix, which are highly variable between different tissues, are known to regulate cell behavior¹⁸.

Is the aggregate composition uniform? It has been shown by numerical simulation that temperature differences in active systems induce phase separation. Similarly, metal MPs immersed in a poorly conductive liquid self-assemble in a strong electrical field due to electrodynamic flow¹⁹.

In the present work, we address the aforementioned questions by means of two experimental approaches. In the first approach, we consider cell aggregates spreading on a glass substrate covered with polystyrene and silica MPs. Strikingly, we observe the activation of the particles by the cells, which became Brownian, and we identify two modes of cell spreading over the carpet of microparticles, “pushing” and “surfing”. In the second approach, we study the formation and the spreading of hybrid aggregates for different volume fractions of polystyrene MPs incorporated within an aggregate. We are able to achieve volume fractions of fluorescent MPs up to 50%. We measure the dynamics of aggregation, and find that microparticles are less efficient cell stickers than nanoparticles. As the microparticle volume fraction increases, aggregate size decreases and the distribution of microparticles inside the aggregate becomes more heterogeneous. Moreover, increasing particle volume fraction slows down the spreading of these hybrid aggregates, which is interpreted as a viscosity increase, indicating that the system is approaching a jamming transition.

Results and discussion

Aggregates and particles. We study in this first part how MPs and cells interact. In particular, we investigate how cell activity

Table 1 List of the microparticles employed.

Microparticles	Material (density)	Diameter [μm] ^a	Functionalization of MPs surface (pH 7.4)
Ps-4.5	Polystyrene (1.05)	4.5	COO ^{-b}
Ps-10	Polystyrene (1.05)	10	COO ⁻
Ps-15	Polystyrene (1.05)	15	COO ⁻
Ps-20	Polystyrene (1.05)	20	COO ⁻
SiO ₂ -1	Silica (2.7)	1.0	COO ⁻
SiO ₂ -5	Silica (2.7)	5.0	COO ⁻
SiO ₂ -10	Silica (2.7)	10.0	COO ⁻
SiO ₂ -20	Silica (2.7)	20.0	COO ⁻

^aProvided by the supplier.
^bCarboxylic acid that is negatively charged at pH 7.4.

induces MP motion. For this purpose, we study how an aggregate of cells spreads on an adhesive substrate in the presence of microparticles.

Microparticles sediment on a glass substrate coated with fibronectin before the addition of cellular aggregates. We used MPs, listed in Table 1, of different sizes (from 1 to 20 μm in diameter) and densities d that are either comparable to the cell's density (polystyrene, $d = 1.05$) or denser than cells (silica, $d = 2.7$).

We define the surface fraction of the MPs as $\Phi_S = v\pi r^2$, where v is the number of MPs per unit area and r the radius of the MPs. A surface fraction $0 < \Phi_S \leq 1$ corresponds to a partially coated substrate. We can also achieve $\Phi_S > 1$, corresponding to surfaces coated with more than one MP layer. Aggregates deposited on the glass substrates decorated with MPs are observed by optical microscopy for at least 15 h. They spread with the formation of a precursor film. The dynamics of aggregate spreading is studied as a function of Φ_S .

Two regimes, internalization and activation, are observed depending on the size and density of the particles. The first regime has been studied previously¹¹. We focus here on the case of particles too large to be phagocytosed.

Substrates decorated with polystyrene MPs. We consider the spreading of a cell aggregate deposited on a bare substrate (Fig. 1a) and on a substrate decorated with polymer MPs (Fig. 1b–e) with a diameter of 4.5, 10, and 20 μm (denoted as Ps-4.5, Ps-10, and Ps-20, respectively). Note that the size of the larger MPs becomes comparable to the cell size.

As observed in Fig. 1, aggregates spread without internalization of the MPs. At the onset of spreading, MPs are pushed away by the cells, forming a MP-free region around the aggregate. They accumulate in a denser zone of MPs at the periphery of the film (Fig. 1b–e). As the cellular agitation is transmitted to the particles, the MPs start to move. For small Φ_S (≤ 0.25), MPs regroup randomly in small clusters along the film periphery, which are very dynamic: they collide, rotate, and exchange MPs (Supplementary Movie 1). The size of the clusters increases with increasing Φ_S , MPs invade the empty region around the aggregate individually or in the form of clusters. By tracking single particles and clusters of MPs, we characterize the time evolution of their position and extract the mean square displacement MSD as a function of time (Supplementary Table 1 and Supplementary Fig. 1). We observe a characteristic two-dimensional diffusive motion, leading to a cluster diffusion coefficient D_{eff} of the order of $10^{-15} \text{ m}^2 \text{ s}^{-1}$. However, in a few cases, particles are trapped in a patch, in analogy to the corral effect introduced to explain the

confined motion of proteins in cell membranes²⁰. Moreover, like Brownian particles, MPs diffuse to equalize their concentration. For large Φ_S (≥ 0.6), they form a dense rim that decomposes into periodic clusters, in analogy with the spinodal decompositions observed in phase separation. Clusters, which can contain several hundred MPs, are highly dynamic and flicker (the fluctuation of particle density modulate the transmitted light, Supplementary Movie 2). At long times (≥ 20 h), clusters invade empty regions (Supplementary Fig. 2) as a manifestation of their Brownian behavior. Taking $D_{\text{eff}} = 10^{-15}$ and $t = 10^5$, we find a length of order 10 μm, comparable to the size of the MP-free region.

Substrates decorated with silica MPs. We now investigate (Fig. 2) the case of silica MPs that have a density much larger than the density of the cells (2.7 compared to 1.05). In this case it is possible to decorate substrates with MPs of size smaller than the minimal size required when using polystyrene MPs because the sedimentation length of silica MPs is ten times smaller¹¹. Here we describe the impact of SiO₂ MPs with diameters d of 1, 5, 10, and 20 μm (denoted as SiO₂- d) on the spreading of cellular aggregates. For 1 μm MPs, cells at the periphery of the spreading monolayer internalize the MPs. This internalization is easily observed by optical microscopy, since cells appear black upon MP internalization (Supplementary Fig. 3). The aggregate spreads and “cleans” very efficiently the substrate, as described previously¹¹. Cells do not internalize larger MPs with sizes of 5, 10 or 20 μm (Fig. 2).

For MPs of size $d = 5$ μm, we observe (Fig. 2a) the formation of an aureole that breaks into clusters in the dilute regime ($\Phi_S \leq 0.25$), same as we described above for polystyrene MPs. The size of the clusters increases with Φ_S . However, for higher concentrations, the MPs are organized in crystalline order. The aggregate spreads now on the dense layer and we no longer see an aureole devoid of MPs forming around the aggregate (Fig. 2b). Instead, flickering appears under the spreading cell monolayer, indicating that the MPs are set into motion underneath the cells. At later time, we observe a phase separation of the activated MPs leading to clusters.

For larger MPs (10 and 20 μm), the polydispersity is higher and there is no appearance of crystalline order, but rather a polycrystalline packing of spheres. However, the behavior is similar. At low densities, clusters form at the periphery of the film (Fig. 2c, d). As soon as the stacking of the MPs is sufficiently compact, aggregates spread on the MP layer. The MPs under the cells are activated and phase separates into clusters, leading to a large region of very heterogeneous particle density around the aggregate (Fig. 2e).

In conclusion, in the regime of dense packing, the cells spread over the “substrate + MPs” system, a behavior that was not observed with light (polystyrene) MPs.

Dynamics of spreading and cluster formation. The dynamics of spreading of aggregates on adhesive substrates is characterized by the spread area $A(t)$ versus time t (Fig. 3a). $A(t)$ is well described by the relationship $(A - A_0)/R_0 = V^*t$ where V^* is a typical velocity, A_0 the area at time $t = 0$ and R_0 the radius of the aggregate⁷. For the spreading on a carpet of lighter (polystyrene) MPs, we have observed a slow-down of the spreading after a characteristic time, as shown on Fig. 3a, d. The rim of MPs becomes very large and gives rise to a resisting force that opposes the spreading of the film. This slowing down is not observed with heavier (silica) MPs (Fig. 3e, f), because aggregates spread on the MPs instead of pushing them into a rim.

We interpret the spreading of the cell monolayer on MPs by an extension of our previous model on a bare substrate¹⁶

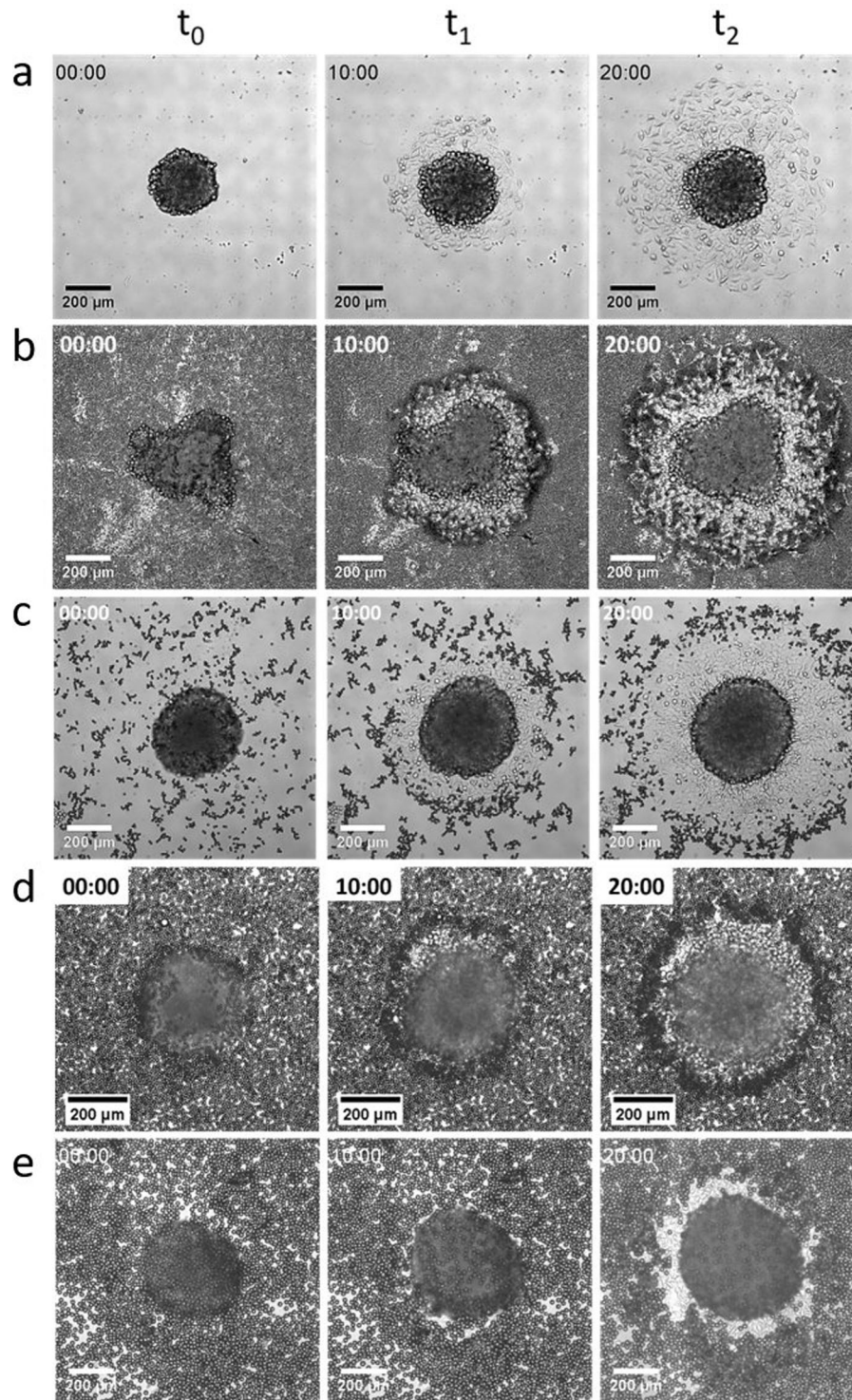


Fig. 1 Cellular aggregates spreading on substrates coated with light polystyrene microparticles. Time-dependent behavior observed in bright-field images of cell aggregates. Aggregates are deposited on (a) a substrate without microparticles (MPs); decorated with polystyrene MPs: b Ps-4.5 with surface fraction $\Phi_S = 0.25$, c Ps-10 with $\Phi_S = 0.13$, d Ps-10 with $\Phi_S = 1.02$, and e Ps-20 with $\Phi_S = 1.02$. Cellular aggregates are the spherical structures in the middle. They spread forming a precursor film made of elongated cells around. MPs are the dark spheres around the precursor film. Time is measured in hours.

including the friction caused by the MP_S . The dynamics of spreading of the precursor film of an aggregate of cells over a bare substrate⁷ were described from the balance between the driving forces S due to the motile cells at the periphery of the film, and the friction forces associated with the permeation flow corresponding to the entry of cells from the aggregates into the

film. This balance leads to

$$2\pi\eta R\dot{R}S = 2\pi\eta \left(\frac{R\dot{R}}{R_L\xi} \right)^2 R_L\xi^2 \cong 2\pi\eta \frac{R^2\dot{R}^2}{R_0}, \quad (1)$$

where η is the aggregate viscosity measured by pipette aspiration,

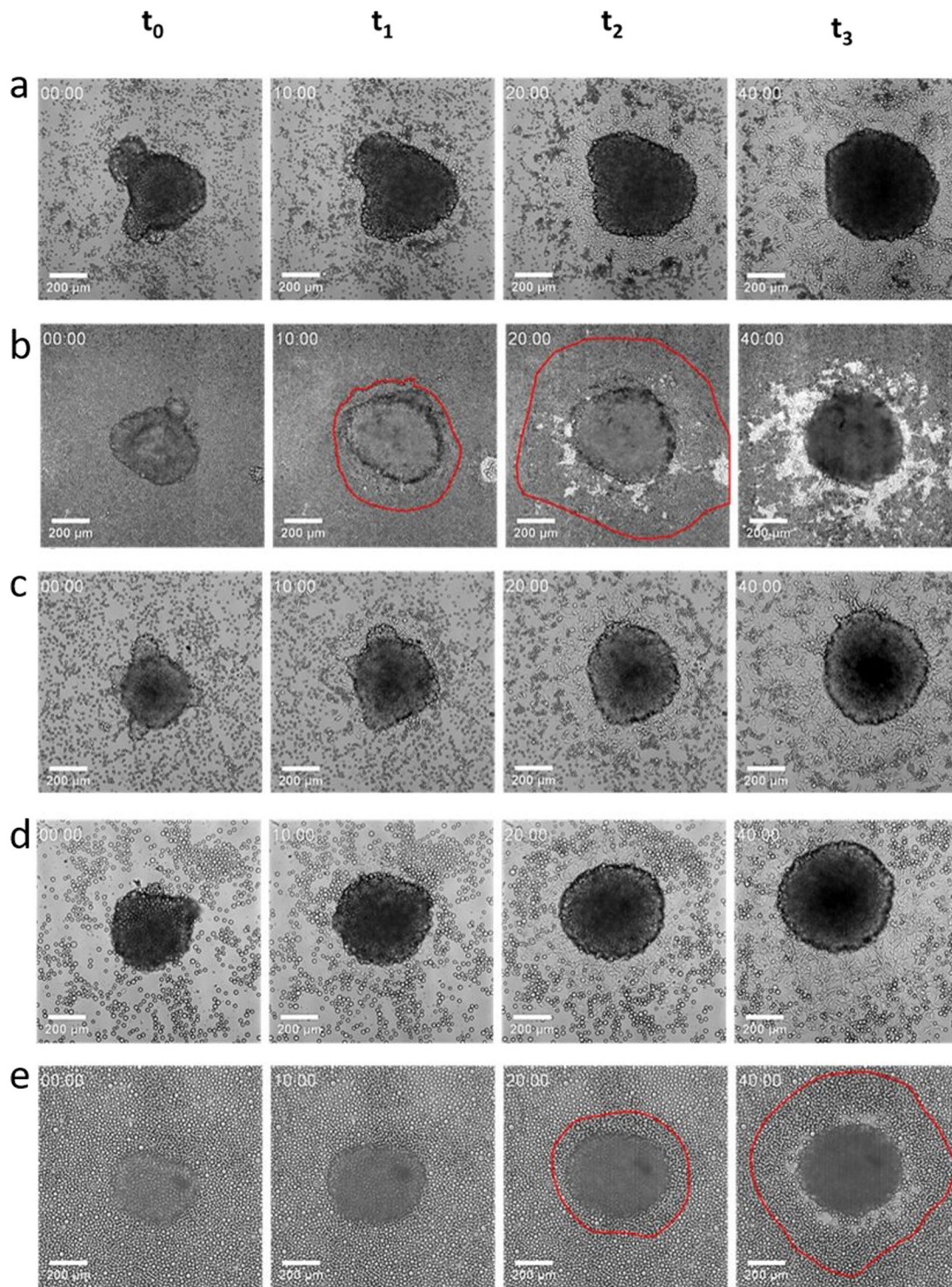


Fig. 2 Cellular aggregates spreading on substrates coated with dense silica microparticles. Bright-field images over time of cell aggregates deposited on substrates decorated with silica microparticles (MPs). **a** SiO₂-5 with surface fraction $\Phi_s = 0.25$, **b** SiO₂-5 with $\Phi_s = 0.76$. **c** SiO₂-10 with $\Phi_s = 0.13$, **d** SiO₂-20 with $\Phi_s = 0.13$, **e** SiO₂-20 with $\Phi_s = 0.96$. Red contours highlight the limit of the cellular film on the layer of silica MPs when difficult to observe. Cellular aggregates are the spherical structures in the middle. They spread forming a precursor film made of elongated cells around. MPs are the spheres around the precursor film. Time is measured in hours.

of the order of $2 \cdot 10^5$ Pa s²¹, R is the radius of the precursor film, R_L is the radius of the contact line between the aggregate and the precursor film, which is nearly equal to the aggregate radius R_0 , $\frac{R\dot{R}}{R_L}$ is the velocity at the contact radius R_L , and ξ is the width of the permeation region. In the following, let us consider how this

description is modified by including the friction due to the MPs.

Spreading of the cell monolayer film pushes the MPs, which form a compact rim. If l is the width of the rim, conservation of particles yields: $2\pi Rl = \pi R^2 \phi_s$, i.e., $2l = R\phi_s$.

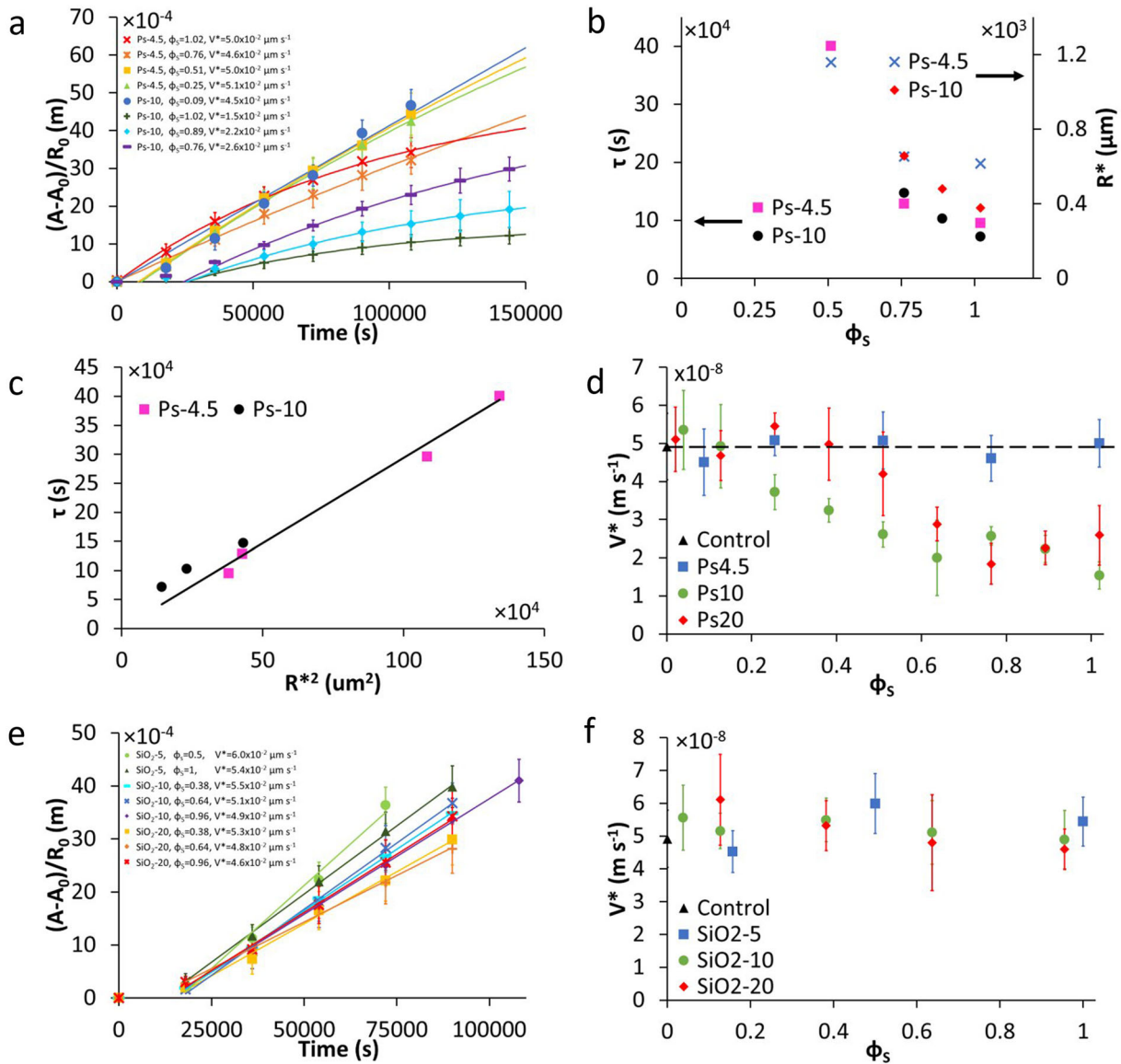


Fig. 3 Characterization of the dynamics of spreading. **a** Spread area versus time for Ps-4.5 microparticles (MPs) and Ps-10 at increasing surface fractions Φ_s . Data are fitted by the theoretical law (Eq. (4)) where V^* is the spreading velocity of cell aggregates. **b** Characteristic time and radius at which spreading stops, as a function of MP surface fraction, for Ps-4.5 and Ps-10. **c** Characteristic time ($\tau = \frac{R^{*2}}{D} = \frac{R^{*2}2\pi}{V^*R_0}$) versus R^{*2} (R^* being the radius at which the spreading stops) for Ps-4.5 and Ps-10. **d** Dynamics of spreading for light polystyrene MPs, where V^* is measured in the linear regime before the spreading slows down. The dashed line highlights V^* of the control cell aggregates for comparison. **e** Spread area versus time for SiO₂ MPs with a diameter of 5, 10, and 20 μm at increasing MP surface fractions. Data are fitted by a linear fit. **f** Dynamics of spreading for heavy silica MPs, where the cells spread on the MPs. V^* is nearly independent upon Φ_s . Error bars represent the standard deviation of $n = 10$ aggregates.

The MPs adhere to the substrate with an adhesion energy W . The force to detach a particle of radius R_p according to the conventional JKR theory of adhesion (the Johnson-Kendall-Roberts) is $\frac{3}{2}\pi WR_p \sim WR_p^{22}$. The viscous loss when the rim of MPs is pushed at a velocity dR/dt proportional to the detachment force per particle and to the number of beads in the rim is given by $WR_p \frac{2\pi Rl}{\pi R_p^2} \dot{R}$.

Adding this term to Eq. (1) leads to:

$$2\pi R \dot{R} S = 2\pi \eta \left(\frac{R \dot{R}}{R_0} \right)^2 R_0 + WR_p \frac{2\pi R l}{\pi R_p^2} \dot{R}, \quad (2)$$

which can be written as:

$$S = \eta \frac{R \dot{R}}{R_0} + S \frac{R}{R^*}, \quad (3)$$

where $R^* = \frac{2\pi R_p S}{W \Phi_s}$ is the radius at which spreading stops because the driving force becomes too weak to push the rim further. In nondimensional units $u = R/R^*$ and $\tilde{t} = t/\tau$, where $\tau = R^{*2}/D$ and $D = SR_0/\eta = V^*R_0/2\pi$, this equation becomes $\frac{u \dot{u}}{1-u} = \frac{d\tilde{t}}{\tau}$.

The general solution is

$$u + \ln(1-u) = \frac{-t + t_0}{\tau}. \quad (4)$$

In the limit $u \rightarrow 0$, the solution can be written as

$$\frac{1}{2}(u^2 - u_0^2) = \frac{t - t_0}{\tau}$$

$$A - A_0 = 2\pi R^{*2} \frac{t - t_0}{\tau} = V^* R_0(t - t_0) \tag{5}$$

In the limit $u \rightarrow 1$,

$$\frac{1 - u}{1 - u_0} = e^{-(t-t_0)/\tau}$$

which leads to

$$\frac{A - A_0}{R_0} = \frac{A^* - A_0}{R_0} \left(1 - e^{-(t-t_0)/\tau}\right). \tag{6}$$

We show the experimental fit (Fig. 3a), which leads to a measurement of R^* and τ . The plot of τ versus the surface fraction of the MPs is shown in Fig. 3b, and τ versus R^{*2} in Fig. 3c. The scaling $V^*R_0\tau = R^{*2}$ is confirmed and the slope of τ versus R^{*2} is equal to $0.3 \text{ s } \mu\text{m}^{-2}$, in agreement with the theoretical value $1/(V^* R_0) = 0.14$. Moreover, we check that R^* vary as Φ_s^{-1} and τ as Φ_s^{-2} (Supplementary Fig. 4).

We propose a simple model to predict the number of particle clusters along the cell aggregate rim. The motion of a cluster is a combination of radial advection, driven by the spreading of the

aggregate, whose radius increases as $R^2 = (V^*/\pi)R_0(t + t_0)$, and diffusion along the periphery of the aggregate, over an arc length $L = R\theta = \sqrt{Dt}$. We suppose that two clusters fusion with each other if they get into contact. Thus, the typical angle between two neighboring clusters scales as θ . By combining the advection and diffusion equations above, we deduce that θ increases over time to reach an asymptotic value in the limit $t \gg t_0$ that scales as $\theta^2 \sim D/(V^*R_0)$.

Hybrid aggregates

In this section, we discuss the case where particles and cells are put into intimate contact forming cell-particle composite materials. We first describe the formation of these hybrid aggregates, obtained by the pendant drop technique, in the absence and presence of MPs. Second, we describe hybrid aggregate spreading.

Dynamics of hybrid aggregate assembly. Hybrid aggregates are prepared using the hanging droplet method (Fig. 4) by mixing cells and MPs to reach the desired composition characterized by $\phi_p = \frac{\text{number of MPs}}{\text{number of MPs} + \text{number of cells}}$, the number fraction of MPs in hybrid cellular aggregates, or by $\phi_v = \frac{\text{volume of MPs}}{\text{volume of MPs} + \text{volume of cells}}$, the volume fraction of microparticles in hybrid cellular aggregates

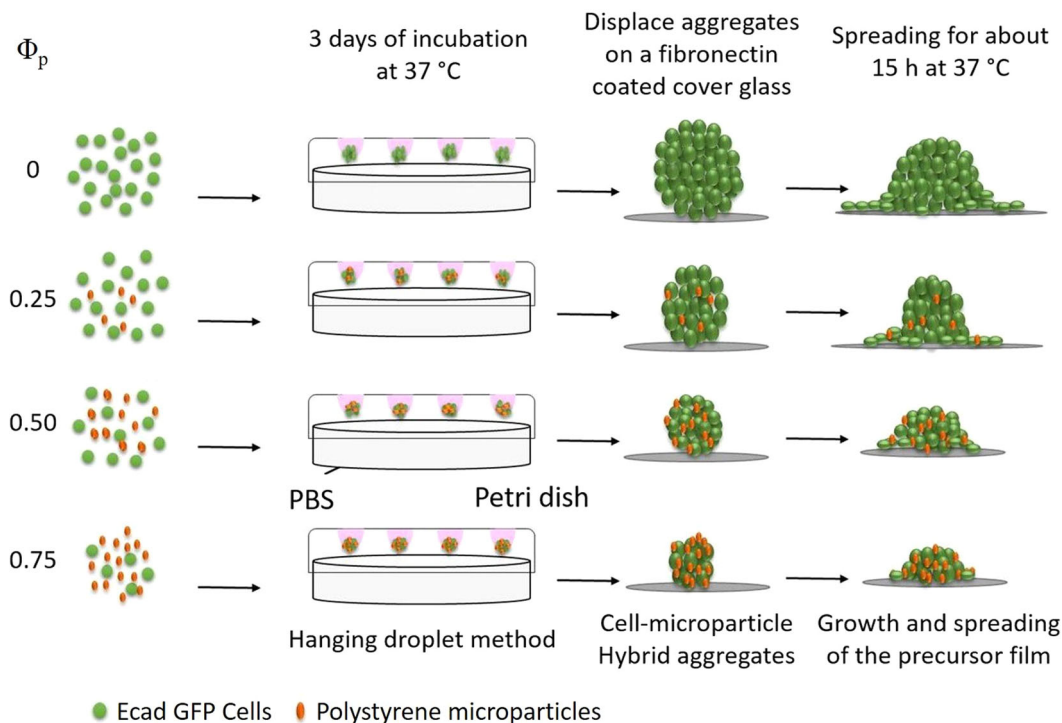


Fig. 4 Graphical representation of formation and spreading of the cell-microparticle hybrid aggregate. Φ_v is the volume fraction of microparticles initially present in the hanging droplets. The total number of cells plus microparticles in each droplet is equal to 3.7×10^4 . Phosphate-buffered saline (PBS) is used to keep Petri dishes humidified.

Volume fraction Φ_v (10 μm)	Volume fraction Φ_v (15 μm)	Number fraction Φ_p	Cell concentration $\times 10^4 \text{ mL}^{-1}$	MPs concentration $\times 10^4 \text{ mL}^{-1}$
0	0	0	3.7	0
0.1	0.29	0.25	2.75	0.925
0.25	0.55	0.5	1.85	1.85
0.5	0.79	0.75	0.925	2.75

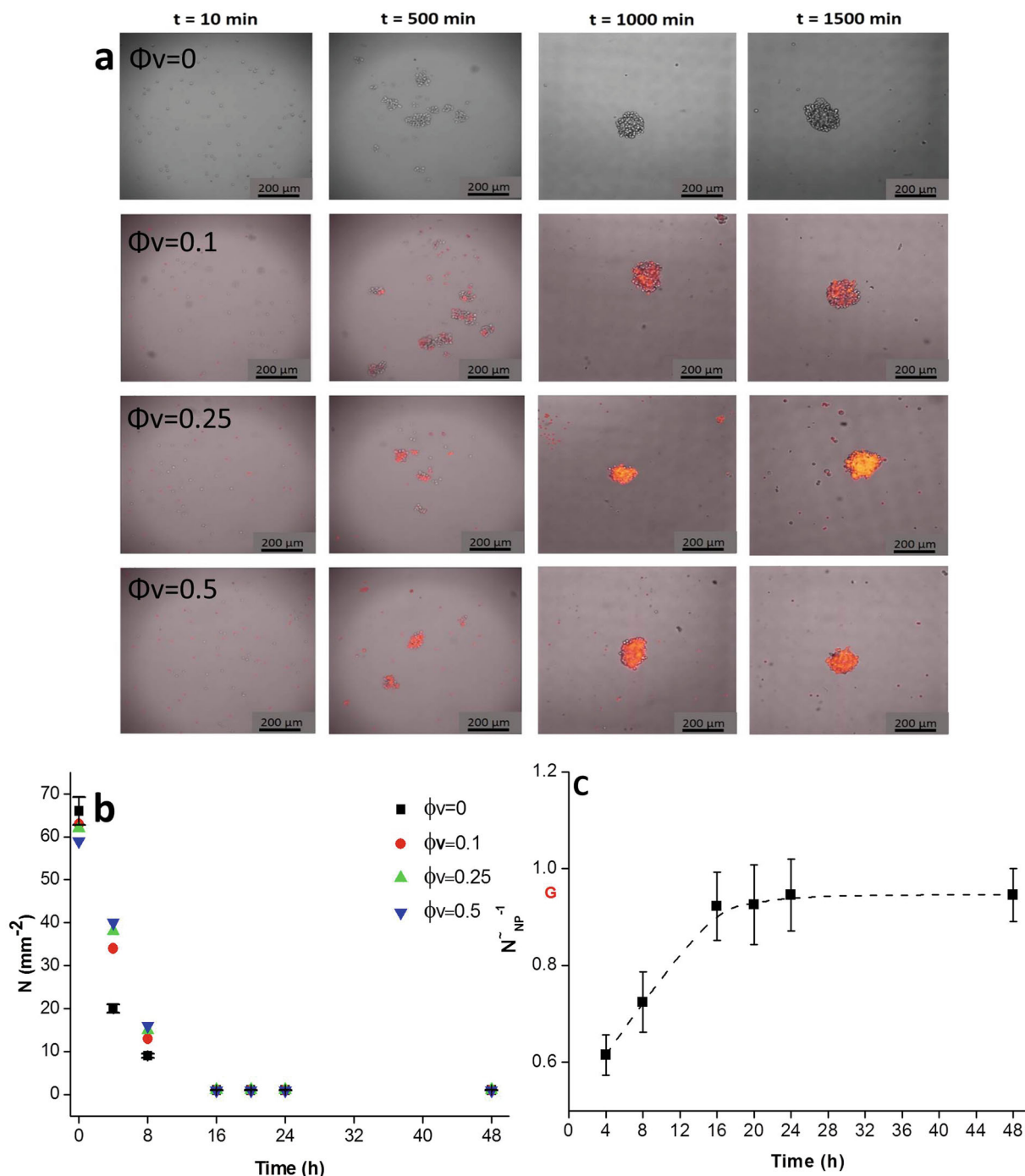


Fig. 5 Formation of hybrid aggregates using the pendant drop method. **a** Optical micrographs of droplets containing Ecad cells and Ps-10 microparticles (MPs) at times 10, 500, 1000 and 1500 min for volume fractions $\Phi_V = 0, 0.1, 0.25$, and 0.5 . **b** Evolution of the number of clusters N per unit area over the incubation time, as counted in optical micrographs of droplets for four Φ_V . **c** Plot of \tilde{N}^{-1} for $\Phi_V = 0.5$, with \tilde{N}^{-1} the ratio of the number of clusters without and with MPs. Error bars represent the standard deviation of $n = 10$ aggregates. G is the efficiency parameter.

maintaining the total number of cells plus beads constant (Table 2). We monitor the number of cell-MP clusters formed, N , as a function of time (Fig. 5a, b).

We have previously studied the dynamics of aggregation of S180 cells, which do not express cadherins, in the presence of polystyrene or silica nanoparticles whose diameter was hundreds of times smaller than that of the microparticles used here¹³. We showed that the number of clusters decreases faster in the presence of nanoparticles, demonstrating that nanoparticles act as cell stickers, replacing the missing cadherins. The time evolution

of the number of clusters $N(t)$ is described by

$$N(t) = N_0 / (1 + N_0 PKt/2),$$

where K is the cluster collision rate and P the probability to stick. The ratio \tilde{N}^{-1} of the number of clusters without and with MPs is defined by $\tilde{N}^{-1} = N_0(t)/N_\Phi(t)$. As shown in Fig. 5c, \tilde{N}^{-1} tends to a limit $G = P_\Phi/P_0$ named the efficiency parameter¹³. We compare the dynamics of aggregation (Fig. 5b) versus the volume fraction Φ_V of Ps-10. With the nanostickers (polystyrene nanoparticles with a diameter of 20 nm), the dynamics of aggregation were

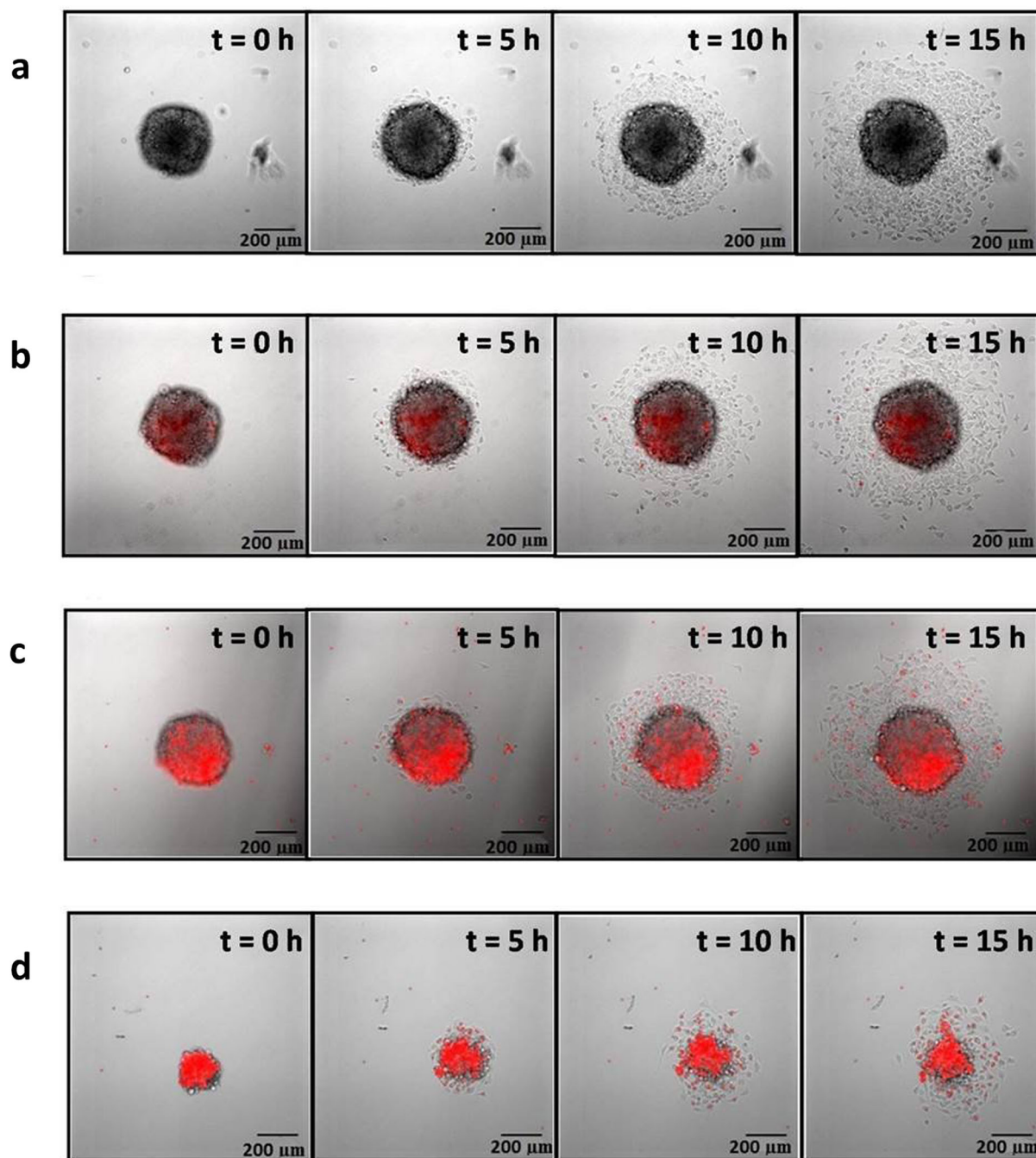


Fig. 6 Spreading of hybrid aggregates for different volume fractions of fluorescent microparticles. **a** The spreading of cell aggregates without microparticles (MPs) as a function of time (volume fraction $\Phi_V = 0$). **b–d** The spreading of cell aggregates as a function of time with Ps-10 MPs (red) volume fractions fixed at $\Phi_V = 0.1, 0.25,$ and 0.5 respectively. We notice that the microparticles are not uniformly distributed and segregation increases with Φ_V .

faster and G was large, up to 5. Here the dynamics is slowed down, as seen in Fig. 5b, G is of the order of 1 (Fig. 5c), albeit slightly smaller. After 3 days of incubation, the hybrid aggregates are formed. Their size $R_M(\Phi_V)$ decreases from 240 to 140 μm as the volume fraction of MPs in hybrid aggregates Φ_V increases from 0 to 0.5 (Supplementary Fig. 5). For volume fractions $\Phi_V > 0.5$, we did not form one aggregate but small clusters. The distribution of beads inside aggregates does not remain uniform as the volume fraction of MPs increases, as shown in Fig. 5a and Supplementary Movies 3 and 4. Toxicity tests (Trypan blue) show

that the viability of cells is not affected by the presence of Ps-10 MPs (Supplementary Fig. 6).

Spreading of aggregates. The hybrid aggregates are deposited on fibronectin-coated surfaces, over which they spread spontaneously. We show in Fig. 6 the spreading of aggregates for different volume fractions (0–0.5) as observed, at given time intervals, by bright-field and epifluorescence microscopy (Fig. 6a–d).

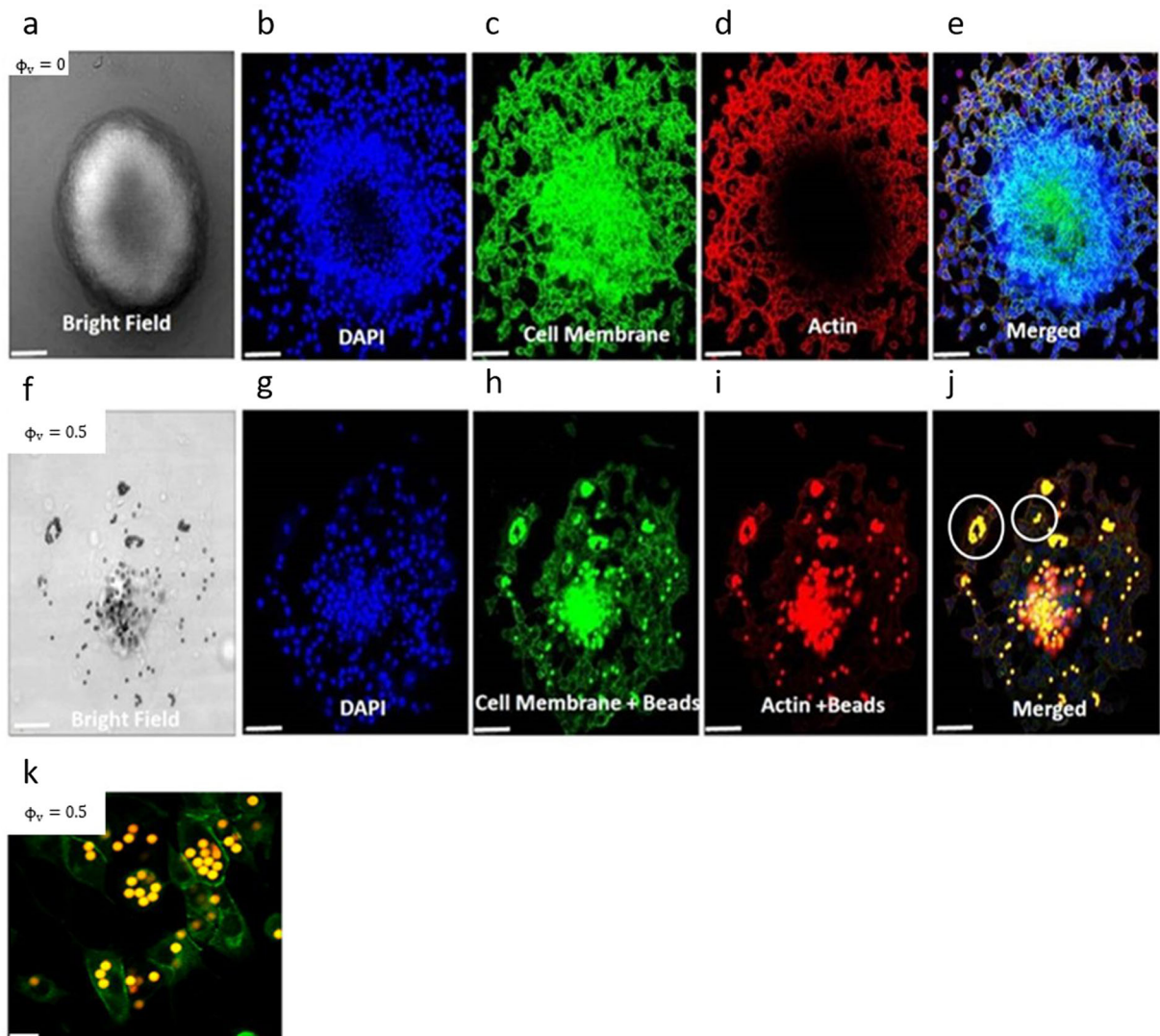


Fig. 7 Bright field and confocal microscopy imaging of spread hybrid aggregates. **a** Bright-field image of a cell aggregate without microparticles (MPs) after spreading for about 24 h. **b–e** Confocal images of the same aggregates with on image **(b)** the fluorescence of the nucleus of the cells using DAPI (4',6-diamidino-2-phenylindole), on the image **(c)** the fluorescence of the cell membrane and MPs, on the image **(d)** the fluorescence of actin and MPs, and on the image **(e)** the fluorescence of merged pictures **(b–d)**. **f** Bright-field image of a cell aggregate with Ps-10 (volume fraction of MPs $\Phi_V = 0.5$) MPs after spreading for about 24 h. **g–j** Confocal images of the same aggregate. **g** The fluorescence of the nucleus of the cells using DAPI, on the image **(h)** the fluorescence of the cell membrane and MPs, on the image **(i)** the fluorescence of actin and MPs, and on the image **(j)** the fluorescence of merged pictures **(b–d)**. The white circles highlight cells that have engulfed several MPs. **k** Zoom of a spread aggregate with Ps-10 ($\Phi_V = 0.5$) after spreading for about 24 h. Scale bars are equal to 100 μm on **(a–j)** and to 25 μm on **(k)**.

In Fig. 6, the red patches correspond to particle-rich regions, where MPs can be either internalized or in clusters. We observe that above a volume fraction of 0.25 the MP distribution inside the aggregates is heterogeneous. This behavior, shown here for MPs with a diameter of 10 μm , is also observed for MPs with a diameter of 15 μm . When studying the spreading of cell aggregates on MPs carpets in “Substrates decorated with silica MPs”, we observed that cells can only internalize small MPs ($d = 1 \mu\text{m}$). The behavior is significantly different in the hybrid aggregates, where MPs that become surrounded by the cells are progressively phagocytosed. MP internalization into cells is observed for all particle sizes studied here. Internalization is demonstrated in Fig. 7, which compares bright-field (Fig. 7a, f) and confocal imaging of spread aggregates with (Fig. 7g–j) and without MPs (Fig. 7b–e). In the hybrid aggregate images, we can see

several MPs of 10 μm internalized into one single cell, whose size became larger as a result (Fig. 7k).

Next, we investigate the dynamics of the spreading of the precursor film surrounding the hybrid aggregate. The measured area of spreading, normalized by the aggregate’s initial radius R_0 , is plotted as a function of time in Fig. 8a–d.

The spreading velocity of hybrid aggregates (derived from Fig. 8 for Ps-10 MPs) versus MP volume fraction is shown in Fig. 9. The decrease of V^* with increasing MP volume fraction can be interpreted as an increase of hybrid aggregate viscosity. To test this hypothesis, we have performed preliminary studies of the mechanical properties of the hybrid aggregates using the micropipette aspiration technique and observed an increase of the aggregate viscosity by a factor 3 when Φ_V increases from 0 to 0.5. When we performed aspiration and retraction cycles, we observed no retraction in some cases, indicating a jamming

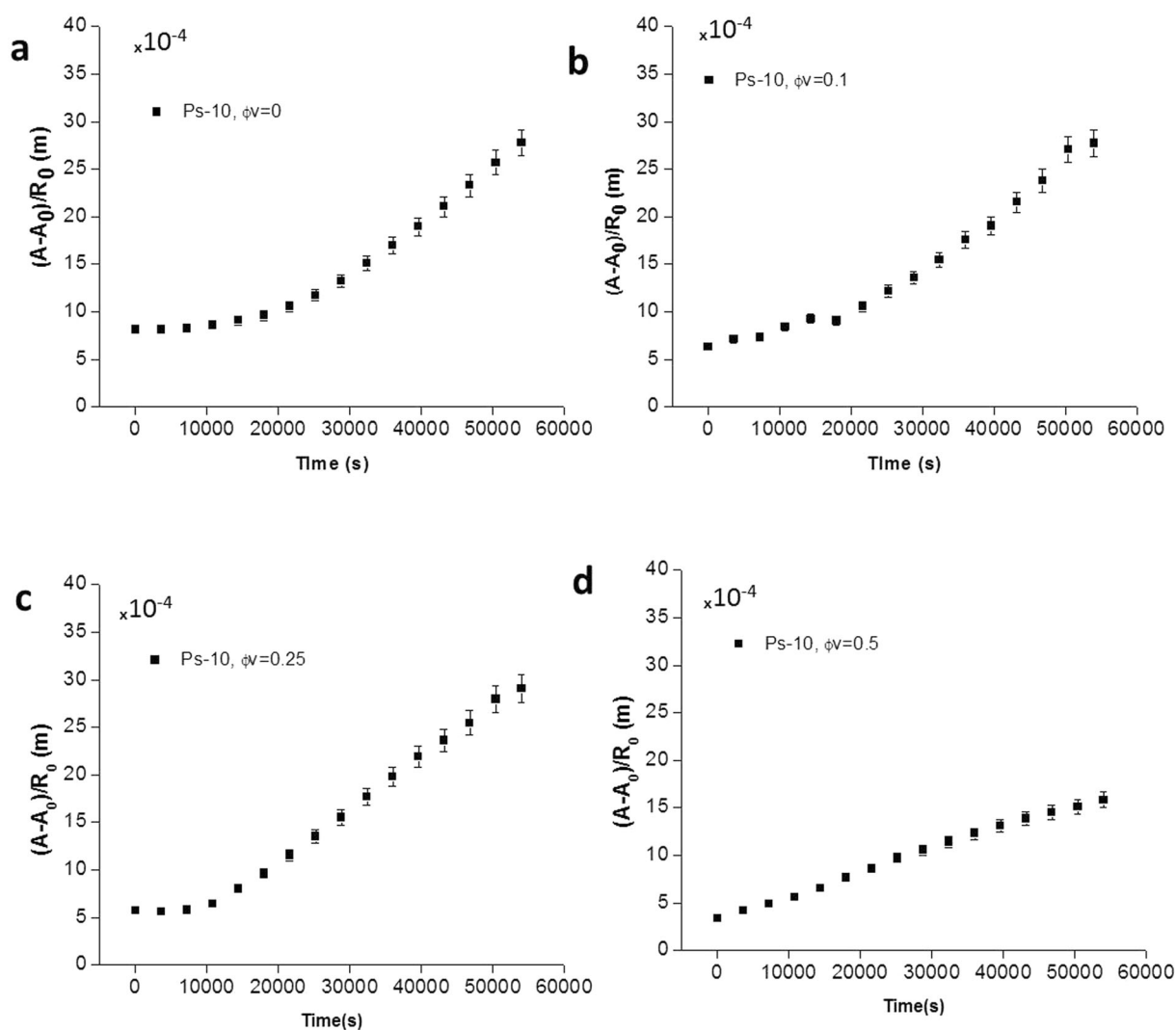


Fig. 8 Dynamics of spreading of hybrid aggregates. Time evolution of the area of the cell monolayer of a hybrid spreading aggregate (formed with Ps-10 MPs) normalized by the initial aggregate radius R_0 . **a** $\Phi_V = 0$ with R_0 ranging from 200 to 285 μm ; **b** $\Phi_V = 0.1$ with R_0 ranging from 150 to 190 μm ; **c** $\Phi_V = 0.25$ with R_0 ranging from 125 to 160 μm , and **d** $\Phi_V = 0.5$ with R_0 ranging from 50 to 110 μm . Error bars represent the standard deviation of $n = 10$ aggregates.

transition in the pipette (Supplementary Fig. 7 and 8). Moreover, for aggregates with a large volume fraction of MPs, we observe a long-time slowdown of the spreading dynamics and $A(t)$ deviates from the linear law (Fig. 8c, d), which can be attributed to a progressive increase of the density of MPs inside the aggregate. Indeed, the density of MPs in the precursor film surrounding the aggregate is smaller than that in the aggregate, as shown in Table 3.

Overall, our results in this section demonstrate that particle volume fraction plays a major role in the spreading velocity of aggregates. We also observe that MP distribution becomes heterogeneous for volume fractions $\phi_V \gtrsim 0.25$. This is an illustration of the phase separation predicted for active systems at two temperatures, “hot” for the cells and “cold” for the particles. Moreover, as for the spreading of binary mixtures, the particle volume fraction in the film and in the aggregate may be different¹⁷.

Conclusion

We have studied how particles interact with cells. In the first part, we have described the spreading of cellular aggregates on a carpet

of MPs of different sizes and densities. We have observed that MPs undergo Brownian-like motion induced by cell-bead collisions. As a result, the MPs diffuse and form cell-MP clusters. This is an example of an “Active granular liquid”, similar to what is also observed in plants. Gravisensors in plant cells consist of starch-rich grains of a few microns that form small granular piles at the bottom of a plant cell. Because of cell activity, gravisensors behave like a liquid and not like a granular material²³.

The interplay between cells and MPs depends upon MP density. For comparable MP and cell densities, cells at the periphery of the spreading monolayer are able to push the light MPs. The MPs accumulate into a rim, which slows down the spreading dynamics and may even halt it. We have proposed a theoretical model to describe the formation of the MP rim and the force that it exerts to oppose aggregate spreading, in good agreement with experimental data. On the other end, if the MPs are heavy, the cells are not able to push the MPs and rather spread above the carpet of MPs. The beads below the cell monolayer are put into motion by the cell activity and form clusters.

In the second part, we have studied the formation of MP-cell aggregates and their spreading dynamics. We have demonstrated

the viability of producing hybrid aggregates with a large volume fraction of MPs, up to 0.5. The dynamics of spreading decreases as the volume fraction of MPs increases, which suggests that the system is approaching a jamming transition. Moreover, the MP distribution becomes heterogeneous, as predicted by numerical simulations that show phase separation in a binary system whose components are at two different temperatures²⁴.

As the aggregate spreads, the density of MPs in the film is smaller than the density in the aggregate. This leak out of cells from the aggregate into the film leads to an aggregate enrichment in MPs,

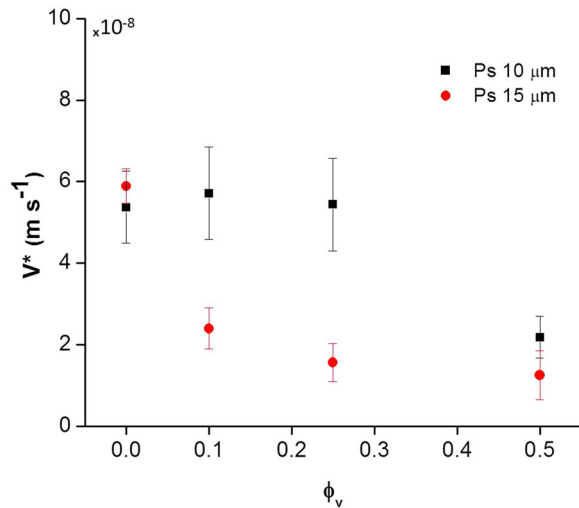


Fig. 9 Spreading velocity of hybrid aggregates as a function of particle volume fraction. Spreading velocity V^* of Ps-10 and Ps-15 microparticles as a function of microparticle volume fraction ϕ_v . Error bars represent the standard deviation of $n = 10$ aggregates.

which may be responsible for the slowing down of the spreading that is observed as the overall MPs volume fraction is increased.

The effects of MPs on the dynamics of cell aggregates may have profound implications on physiological processes such as cancer metastasis and development. In the future, it would be interesting to extend this work to jelly soft particles, to mimic the role of the extracellular matrix.

Methods

Materials. Fibronectin and phosphate-buffered saline (PBS) were purchased from Sigma-Aldrich Co. Trypsin-EDTA, penicillin-streptomycin, Dulbecco’s Modified Eagle Medium (DMEM), and polystyrene MPs 10 and 15 μm in diameter (Fluo-Spheres®) were obtained from Life Technologies Co. Polystyrene MPs 20 μm (Polybead®) and 4.5 μm (Fluoresbrite®) in diameter were obtained from Polysciences Co. Silica MPs were obtained from Corpuiscular, Co.

Cell culture and aggregates preparation. We used murine sarcoma (S180) cells transfected to express E-cadherins molecules on their surface²⁵, which were a generous gift from Dr. Sylvie Dufour (INSERM, U955, France). In some of the pipette aspiration experiments we used a variation of the cell same line transfected to express a larger amount of E-cadherins (twice the amount)¹⁶. Unless indicated otherwise, cells used in this study are those of the first type. Cells were cultured at 37 °C under a 95% air/5% CO₂ atmosphere in a culture medium consisting of DMEM supplemented with 10% (v/v) fetal bovine serum (FBS) and antibiotics (100 μm mL⁻¹ streptomycin and 100 U mL⁻¹ penicillin).

Cell/MP aggregates were prepared using a modified hanging droplet method (Fig. 4). Upon reaching confluence, cells were detached from the flask using trypsin and dispersed into DMEM with a concentration of 4×10^5 cells mL⁻¹. MPs were added to the cells to reach the desired concentration (3.7×10^4 cells mL⁻¹) by varying the number fraction Φ_p of MPs ($\Phi_p = \frac{\text{number of MPs}}{\text{number of MPs} + \text{number of cells}} = 0, 0.25, 0.5, \text{ and } 0.75$, respectively). The corresponding volume fractions, defined as $\Phi_v = \frac{\text{volume of MPs}}{\text{volume of MPs} + \text{volume of cells}}$ and calculated by taking a volume per single cell equal to 1600 μm^3 , are indicated in Table 2.

Droplets (15 μL) of the cell/MP suspension in cell culture medium were deposited on the lid of a Petri dish. The lid was inverted and placed on top of a Petri dish filled with PBS, such that the droplets containing the cells in the medium and hanging from the lid were maintained under a high humidity atmosphere. Due to gravity, cells fell to the bottom of the droplets and started to adhere to each other

Table 3 Repartition of microparticles and cells in aggregates at different stages.

Volume fraction Φ_v		0	0.1	0.25	0.5								
Number of objects added in the aggregate formation (in a hanging drop)	Cells	555	413	278	138								
	Beads	-	138	278	413								
Total number of objects in each aggregate after 3 days of incubation (before spreading)	Cells	766	499	412	211								
	Beads	-	85	130	310								
Repartition of objects (after spreading)		In core	In film	%	In core	In film	%	In core	In film	%	In core	In film	%
Total number of objects in each aggregate (after spreading)	Cells	496	584		400	432		333	388		130	176	
	Beads	-	-		60	10		146	35		227	55	
Number of beads in I quarter	Cells	126	147	24	141	155	33	95	111	28	38	52	29
	Beads	-	-		20	3		42	10		66	16	
Number of beads in II quarter	Cells	124	155	22	51	72	15	78	91	23	36	48	27
	Beads	-	-		9	2		34	8		63	15	
Number of beads in III quarter	Cells	117	142	27	117	142	30	72	83	21	26	35	20
	Beads	-	-		18	3		31	8		46	11	
Number of beads in IV quarter	Cells	129	140	27	91	98	21	88	103	26	30	41	23
	Beads	-	-		13	2		39	9		52	13	
$\Phi_p = \frac{\text{number of MPs}}{\text{number of MPs} + \text{number of cells}}$	In a hanging drop			$\Phi_p = 0.25$			$\Phi_p = 0.5$			$\Phi_p = 0.75$			
	(Assuming all beads in an aggregate)			$\Phi_v = 0.1$			$\Phi_v = 0.25$			$\Phi_v = 0.5$			
$\Phi_v = \frac{\text{number of MPs} \cdot V_p}{\text{number of MPs} \cdot V_p + \text{number of cells} \cdot V_c}$	Before Spreading			$\Phi_p = 0.15$			$\Phi_p = 0.24$			$\Phi_p = 0.59$			
	(3 days of incubation)			$\Phi_v = 0.05$			$\Phi_v = 0.09$			$\Phi_v = 0.32$			
	After Spreading	Core		$\Phi_p = 0.13$			$\Phi_p = 0.30$			$\Phi_p = 0.64$			
		Film		$\Phi_v = 0.05$			$\Phi_v = 0.12$			$\Phi_v = 0.37$			
				$\Phi_p = 0.02$			$\Phi_p = 0.08$			$\Phi_p = 0.24$			
				$\Phi_v = 0.01$			$\Phi_v = 0.03$			$\Phi_v = 0.09$			

$n = 5$ aggregates with Ps-10 microparticles (MPs) are measured as hanging droplets, before, and after spreading. Aggregates are assumed to be spherical and divided in four Quarters for the measure.

to form clusters of cells. After 3 days of incubation at 37 °C under a 95% air/5% CO₂ atmosphere, cell aggregates were formed. For experiments with cells alone ($\Phi_V = 0$), the same protocol was followed except that the addition of MPs was omitted.

Preparation of coated glass substrates for cellular assays. Twenty-five millimeters circular glass coverslips were sonicated in ethanol for 5 min, dried at ambient temperature, and exposed to deep UV for 5 min. The coating was performed using a 0.1 mg mL⁻¹ solution of fibronectin in PBS at pH 7.4 for 1 h.

Aggregate spreading assays and optical microscopy. A cylindrical sample cell (magnetic chamber, Chamliide Co.) suitable for use with an inverted optical microscope (Zeiss Axiovert 100 equipped with a 10× 0.45 objective or Leica TIRF AF 6000LX, equipped with a 10× 0.30 objective) was fitted with a fibronectin-coated glass coverslip, which formed the bottom of the sample chamber. The chamber was filled with CO₂-equilibrated culture medium, consisting of DMEM supplemented with 10% (vol/vol) FBS and antibiotics (100 μ mL⁻¹ streptomycin and 100 U mL⁻¹ penicillin), maintained at 37 °C using a temperature-controlled platform. For experiments of cellular aggregates spreading on carpets of MPs, MPs with the desired diameter were added to the chamber to obtain the required surface fraction. MPs were let to settle for a few minutes, so that they deposited on the substrate of the chamber, except in the case of SiO₂-1 and Ps-4.5 where the sample chamber was kept in the incubator overnight. For hybrid cell-MP aggregates at $\Phi_S = 0$, no MPs are added (Fig. 4). Aggregates were then introduced into the sample chamber, and the open surface was sealed with mineral oil to prevent water evaporation. Bright-field images were taken at time intervals of 10 min for at least 15 h. Images were exported from the instrument software in TIFF format and visualized using the ImageJ software package v.1.46r (National Institutes of Health, Bethesda, MD).

2D diffusion analysis. During the spreading experiments of cell aggregates on carpets of MPs, the diffusion of single or clusters of MPs (Ps-4.5 or Si-5) in the film of cells was studied by determining their Mean-Square displacement (MSD)²⁶. $MSD(t) = \frac{1}{N-\alpha+1} \sum_{i=0}^{N-\alpha} \left\{ [x(t_{i+\alpha}) - x(t_i)]^2 + [y(t_{i+\alpha}) - y(t_i)]^2 \right\}$ for a time increment $t = \alpha\delta t$, where $x(t_i)$ and $y(t_i)$ are the Cartesian coordinates of the successive positions of the MPs at discrete observation times t_0, t_1, \dots, t_N separated by δt : $t_i = i\delta t$ ($\delta t = 10$ min). From the slope of the curve the diffusion coefficient was extracted by applying the relationship $Slope = 4D_{eff}$.

Pipette aspiration. The method and the set-up of the technique have been described elsewhere^{21,27}.

Micropipettes are prepared by pulling borosilicate capillaries (1 mm/ 0.5 mm outer/inner diameter) using a puller (PN-31, Narishige) and sized to the desired inner diameter using a microforge (MF-900, Narishige). The pipettes are then sterilized in a UV plasma chamber and incubated in 0.1 mg/mL Polyethylene glycol polylysine (PLL(20)-g[3.5]-PEG(2), SuSoS AG) in a HEPES solution (pH 7.3) for 1 h, to prevent cell adhesion to the micropipettes. The pipettes are connected through tubings to a water tank of controllable height and then filled with water. The observation chamber is a Petri dish (60 mm × 15 mm) poured with CO₂ equilibrated culture medium. Aggregates and the micropipette are then introduced into the Petri dish. The Petri dish is then sealed with mineral oil to prevent evaporation of the medium and release of CO₂. The micropipette is brought into contact with an aggregate and a suction pressure is applied by vertically moving the water tank. For ΔP larger than a threshold pressure ΔP_c , the aggregates are sucked into the pipette, forming a tongue of length $L(t)$. Aspirated cellular aggregates are visualized with an inverted microscope (Zeiss Axiovert 100 equipped with a ×10 0.30 objective). Bright-field images are recorded with a CCD camera (Photometrics Cascade 512B, Roper Scientific) at a time interval of 5 or 10 s. All the experiments are performed at 37 °C.

Cell viability. Cell viability in aggregates was checked using the Trypan blue dye exclusion test (Supplementary Fig. 6). After letting the aggregate spread for 15 h, Trypan blue was added to the experimental chamber to a final concentration of 0.1% for 10 min.

Data availability

All data needed to evaluate the conclusions in the paper are present in the paper and/or the Supplementary Information. The data that support the findings of this study are available from the corresponding author upon reasonable request.

Received: 27 April 2020; Accepted: 26 November 2020;

Published online: 04 January 2021

References

- Hu, D. L., Phonekeo, S., Altshuler, E. & Brochard-Wyart, F. Entangled active matter: from cells to ants. *Eur. Phys. J. Spec. Top.* **225**, 629–649 (2016).
- Bissell, M. J., Rizki, A. & Mian, I. S. Tissue architecture: the ultimate regulator of breast epithelial function. *Curr. Opin. Cell Biol.* **15**, 753–762 (2003).
- Moscona, A. The development in vitro of chimeric aggregates of dissociated embryonic chick and mouse cells. *Proc. Natl Acad. Sci. USA* **43**, 184–194 (1957).
- Sutherland, R. M., McCredie, J. A. & Inch, R. W. Growth of multicell spheroids in tissue culture as a model of nodular carcinomas. *J. Natl Cancer Inst.* **46**, 113–120 (1971).
- Ryan, P. L., Foty, R. A., Kohn, J. & Steinberg, M. S. Tissue spreading on implantable substrates is a competitive outcome of cell-cell vs. cell-substratum adhesivity. *Proc. Natl Acad. Sci. USA* **98**, 4323–4327 (2001).
- Gonzalez-Rodriguez, D., Guevorkian, K., Douezan, S. & Brochard-Wyart, F. Soft matter models of developing tissues and tumors. *Science* **338**, 910–917 (2012).
- Beaune, G. et al. How cells flow in the spreading of cellular aggregates. *Proc. Natl Acad. Sci. USA* <https://doi.org/10.1073/pnas.1323788111> (2014).
- Duguay, D., Foty, R. A. & Steinberg, M. S. Cadherin-mediated cell adhesion and tissue segregation: qualitative and quantitative determinants. *Dev. Biol.* **253**, 309–323 (2003).
- Foty, R. A. & Steinberg, M. S. The differential adhesion hypothesis: a direct evaluation. *Dev. Biol.* **278**, 255–263 (2005).
- Stenhammar, J., Tiribocchi, A., Allen, R. J., Marenduzzo, D. & Cates, M. E. Continuum theory of phase separation kinetics for active Brownian particles. *Phys. Rev. Lett.* **111**, 145702 (2013).
- Beaune, G., Lam, A. Y. W., Dufour, S., Winnik, F. M. & Brochard-Wyart, F. How glutinous cell aggregates clear substrates coated with microparticles. *Sci. Rep.* **7**, 15729 (2017).
- Wu, X.-L. & Libchaber, A. Particle diffusion in a quasi-two-dimensional bacterial bath. *Phys. Rev. Lett.* **84**, 3017–3020 (2000).
- Brunel, B. et al. Nanostickers for cells: a model study using cell-nanoparticle hybrid aggregates. *Soft Matter* **12**, 7902–7907 (2016).
- Mongera, A. et al. A fluid-to-solid jamming transition underlies vertebrate body axis elongation. *Nature* **561**, 401–405 (2018).
- Tabdanov, E. D. et al. Bimodal sensing of guidance cues in mechanically distinct microenvironments. *Nat. Commun.* **9**, 4891 (2018).
- Douezan, S. et al. Spreading dynamics and wetting transition of cellular aggregates. *Proc. Natl Acad. Sci. USA* **108**, 7315–7320 (2011).
- Brochard-Wyart, F., Fondécave, R. & Boudoussier, M. Wetting of antagonist mixtures: the ‘leak out’ transition. *Int. J. Eng. Sci.* **38**, 1033–1047 (2000).
- Daley, W. P., Peters, S. B. & Larsen, M. Extracellular matrix dynamics in development and regenerative medicine. *J. Cell Sci.* **121**, 255–264 (2008).
- Sapozhnikov, M. V., Tolmachev, Y. V., Aranson, I. S. & Kwok, W.-K. Dynamic self-assembly and patterns in electrostatically driven granular media. *Phys. Rev. Lett.* **90**, 114301 (2003).
- Saxton, M. J. Single-particle tracking: effects of corrals. *Biophys. J.* **69**, 389–398 (1995).
- Guevorkian, K., Colbert, M.-J., Durth, M., Dufour, S. & Brochard-Wyart, F. Aspiration of biological viscoelastic drops. *Phys. Rev. Lett.* **104**, 218101 (2010).
- Johnson, K. L., Kendall, K. & Roberts, A. D. Surface energy and the contact of elastic solids. *Proc. R. Soc. A Math. Phys. Eng. Sci.* **324**, 301–313 (1971).
- Bérut, A. et al. Gravisensors in plant cells behave like an active granular liquid. *Proc. Natl Acad. Sci. USA* **115**, 5123–5128 (2018).
- Stenhammar, J., Wittkowski, R., Marenduzzo, D. & Cates, M. E. Activity-induced phase separation and self-assembly in mixtures of active and passive particles. *Phys. Rev. Lett.* **114**, 018301 (2015).
- Chu, Y.-S. et al. Force measurements in E-cadherin-mediated cell doublets reveal rapid adhesion strengthened by actin cytoskeleton remodeling through Rac and Cdc42. *J. Cell Biol.* **167**, 1183–1194 (2004).
- Douezan, S. & Brochard-Wyart, F. Active diffusion-limited aggregation of cells. *Soft Matter* **8**, 784 (2012).
- Khalifat, N., Beaune, G., Nagarajan, U., Winnik, F. M. & Brochard-Wyart, F. Soft matter physics: tools and mechanical models for living cellular aggregates. *Jpn. J. Appl. Phys.* **55**, 1102A8 (2016).

Acknowledgements

This study was supported by the NIMS Molecule & Material Synthesis Platform of the “Nanotechnology Platform Project” and the World Premier International Research Center Initiative (WPI), both operated by the Ministry of Education, Culture, Sports, Science and Technology (MEXT), Japan. The authors acknowledge the financial

support from the Laboratoire d'Excellence Cell(n)Scale, CeTisPhyBio and PIC3D of the Institut Curie. ANR-10-LBX-0038 is part of the IDEX Idex PSL ANR-10-IDEX-0001-02 PSL.

Author contributions

G.B., F.M.W., and F.B.-W. designed the research, D.G.-R. and F.B.-W. completed the theoretical work, U.N., G.B., and A.Y.W.L. performed the experiments, U.N., G.B., D.G.-R., and F.B.-W. contributed to the writing of the paper and all authors agreed the final content of the paper.

Competing interests

The authors declare no competing interests.

Additional information

Supplementary information is available for this paper at <https://doi.org/10.1038/s42005-020-00506-y>.

Correspondence and requests for materials should be addressed to F.B.-W.

Reprints and permission information is available at <http://www.nature.com/reprints>

Publisher's note Springer Nature remains neutral with regard to jurisdictional claims in published maps and institutional affiliations.



Open Access This article is licensed under a Creative Commons Attribution 4.0 International License, which permits use, sharing, adaptation, distribution and reproduction in any medium or format, as long as you give appropriate credit to the original author(s) and the source, provide a link to the Creative Commons license, and indicate if changes were made. The images or other third party material in this article are included in the article's Creative Commons license, unless indicated otherwise in a credit line to the material. If material is not included in the article's Creative Commons license and your intended use is not permitted by statutory regulation or exceeds the permitted use, you will need to obtain permission directly from the copyright holder. To view a copy of this license, visit <http://creativecommons.org/licenses/by/4.0/>.

© The Author(s) 2021